JGR Earth Surface

RESEARCH ARTICLE
10.1029/2018JF004975

Disentangling and Parameterizing Shallow Sources of Subsidence: Application to a Reclaimed Coastal Area, Flevoland, the Netherlands

Peter A. Fokker[1,2], Jan L. Gunnink[3], Kay Koster[3], and Ger de Lange[4]

[1]TNO Applied Geoscience, Utrecht, Netherlands, [2]University of Utrecht, Utrecht, Netherlands, [3]TNO—Geological Survey of the Netherlands, Utrecht, Netherlands, [4]Deltares, Utrecht, the Netherlands

Key Points:
- Annual subsidence measurements were used for compression parameter estimation
- An Ensemble Smoother with Multiple Data Assimilation was employed
- Shrinkage of clay and organic clay was found the main contributor to compression

Supporting Information:
- Supporting Information S1
- Table S1

Correspondence to:
P. A. Fokker,
peter.fokker@tno.nl

Citation:
Fokker, P. A., Gunnink, J. L., Koster, K., & de Lange, G. (2019). Disentangling and parameterizing shallow sources of subsidence: Application to a reclaimed coastal area, Flevoland, the Netherlands. *Journal of Geophysical Research: Earth Surface*, *124*, 1099–1117. https://doi.org/10.1029/2018JF004975

Received 10 DEC 2018
Accepted 8 APR 2019
Accepted article online 16 APR 2019
Published online 2 MAY 2019

Abstract The natural surface area of many coastal and delta plains has been increased by land reclamation in response to growing populations. These reclaimed lands are often experiencing subsidence. The reclaimed South Flevopolder in the coastal plain of the Netherlands has experienced severe subsidence after its reclamation in 1968. The subsidence is caused by phreatic groundwater level lowering and the associated aeration of the former subaqueous shallow subsurface and increased effective stresses. In this study, surface elevation measurements that quantify the subsidence, conducted annually between 1968 and 1993, and in 2009 and 2012, have been used to constrain and estimate the parameters in models that describe subsidence. For the estimation an Ensemble Smoother with Multiple Data Assimilation was employed. For the forward models, we employed correlations for compression (primary consolidation and creep), oxidation, and shrinkage of coastal deposits. Shrinkage of the aerated clay and organic clay layers was found to be the main contributor to subsidence, and the measurements could be represented well. The quantification of the model parameters allows for better subsidence forecasts. The stochastic method that was employed further facilitates to define a quality measure for forecasts in terms of a covariance matrix or a confidence range.

1. Introduction

Many coastal and delta plains are heavily populated because they provide fertile grounds for agriculture and fresh water for domestic and industrial use and are consequently important economic zones (Day et al., 2016; Renaud et al., 2013). To accommodate growing populations in these areas and to increase the areal of fertile grounds and freshwater reservoirs, the natural surface area of multiple coastal and deltaic plains has in recent times been artificially extended by land reclamations (e.g., Abd El-Kawy et al., 2011; Chena & Zong, 1999; Zhao et al., 2011). Reclaimed areas, however, are often experiencing land subsidence after reclamation (e.g., Auerbach et al., 2015; Drexler et al., 2009; Gambolati et al., 2006). This counter effects their initial purpose, as it may result in saline groundwater intrusion, damage to infrastructure, and increased flood risks. Therefore, subsidence threatens the viability and economic value of these low-lying artificially obtained areas.

The Netherlands has a circa 400-year-old tradition of reclaiming coastal and deltaic lands, which are referred to as "polders". One of the largest polders is the South Flevoland polder (approximately 430 km^2), which was reclaimed in 1968. It has experienced 1 to 2 m of subsidence caused by compression and shrinkage of clay and peat layers and by oxidation of peat layers. The main driver for these processes is phreatic groundwater level lowering due to human intervention. Because ongoing human intervention of groundwater management is required to prevent the South Flevoland polder from inundating, the area will continue to subside. Being able to forecast the absolute value of the subsidence and its spatial variability is crucial to identify the areas that are most affected by subsidence and to propose measures to counteract the adverse effects of subsidence.

Subsidence models are generally based on field and laboratory measurements (e.g., Schothorst, 1982; Van Asselen et al., 2018), sometimes incorporating a physical basis to describe the underlying subsidence processes (e.g., Gambolati et al., 2006; Koster, Stafleu, & Stouthamer, 2018; Van der Meulen et al., 2007). However, model outcomes are critically dependent on model parameters, soil parameters, and the drivers that cause the subsidence. A match between model outcomes and historic data is thus a prerequisite for accurate forecasts. A parameter estimation procedure can then be employed to improve the knowledge

about these parameters. Often, a trial-and-error history matching technique is used [see, e.g., Teatini et al., 2006, Castellazzi et al., 2016], but it is considered more efficient to employ a mathematically based technique. As an example, Bakr (2015) used a maximum likelihood technique for estimation of soil compression parameters in the Jakarta area. However, the drawback of this method is that it does not explicitly deliver the uncertainty of the estimated parameters, which makes it difficult to assess the robustness of decisions based on estimates which are derived with the updated parameters. Li et al. (2017) used an Ensemble Kalman Filter to show the strength of ensemble techniques. They focused on the implementation of the data assimilation and the assessment of flow properties, using a synthetic case study in which little attention was given to the subsidence models. Peduto et al. (2016) used a stochastic technique for the assimilation and prediction of settlement of a railway which did allow quantification of a forecast confidence bound. The latter two examples are implementations of the data assimilation technology that has been applied widely in many disciplines, including groundwater flow and subsurface modelling (Evensen, 2009), but is not yet very common in interpreting shallow causes of subsidence.

In the South Flevoland polder, annual surface elevation measurements were conducted between 1968 (directly after reclamation) and 1993. An additional elevation measurement campaign was conducted in 2012. Furthermore, detailed airborne Lidar images were produced in 2009. Therefore, an extensive data set describing historic surface elevation changes in the South Flevoland polder for a time period spanning almost half a century is available.

The research described here targets the determination of model parameters for subsidence modelling and the quantification of the contributions of the different subsurface processes, by using these measured data in South Flevoland. The approach consists of a data assimilation technique. We used an ensemble technique which outputs an updated distribution of forecasts. We wish to demonstrate the usefulness of this procedure in terms of parameter estimation potential and in terms of its ability to assess the quality of the result. The latter is formulated as expected distribution bandwidth of the model and robustness of decisions based on it.

We identified the major contributors to subsidence and obtained model parameters for three processes: compression, oxidation, and shrinkage caused by phreatic groundwater level lowering. Of these three, shrinkage had been added as an additional process to the traditionally used other two in the Netherlands (e.g., Koster, Stafleu, & Stouthamer, 2018; Muntendam-Bos et al., 2009; Nieuwenhuis & Schokking, 1997; Van der Meulen et al., 2007), because the study area consists of reclaimed subaqueous deposits in which first-time groundwater lowering might induce a compaction mechanism in fine grained soil that would not otherwise be accurately represented (e.g., Doornkamp, 1993).

Shrinkage of clay is a generally acknowledged process that results in volumetric loss of subsurface layers during aeration (Bronswijk, 1989). This especially accounts for clay layers formed in subaqueous environments. In the Netherlands, shrinkage used to be considered as one of the prime contributors to land subsidence in clay-rich agricultural areas (De Glopper, 1969, 1984; Schothorst, 1977, 1982). Nevertheless, in tandem with international developments, the focus of shallow subsidence investigations shifted toward peat areas in the 1990s, as these emit greenhouse gasses during the process of oxidation (Nieuwenhuis & Schokking, 1997). This led to a knowledge gap regarding the contribution of clay shrinkage to total subsidence in the Netherlands. Consequently, an earlier study in which we attempted to match the data without the inclusion of shrinkage failed (Fokker et al., 2015). The present study has reintroduced the phenomenon and shows its importance in understanding subsidence in reclaimed land.

2. Study Area

The South Flevoland polder is situated in the center of the Netherlands, at the landward margin of a Holocene coastal plain, offshore the inland IJssel River delta (Figure 1). The coastal plain formed during Middle to Late Holocene (ca. 7,000- to 5,000-year before present, BP) transgression onlapping a Pleistocene surface (Vos, 2015). The coastal sequence is between <1 and 10 m in thickness and primarily consists of alternating clay and peat layers, which are interfingering with sand. The base of the sequence primarily consists of peat. The transgression gradually transformed this peatland into a tidal basin. The western part of the study area was situated in the most distal part of the tidal basin. Consequently, clay locally alternating with sandy deposits is overlying the peat layer in that part. The eastern inland part of the study area received little sediments from the tidal basins, and several meters of peat sequences could form in a

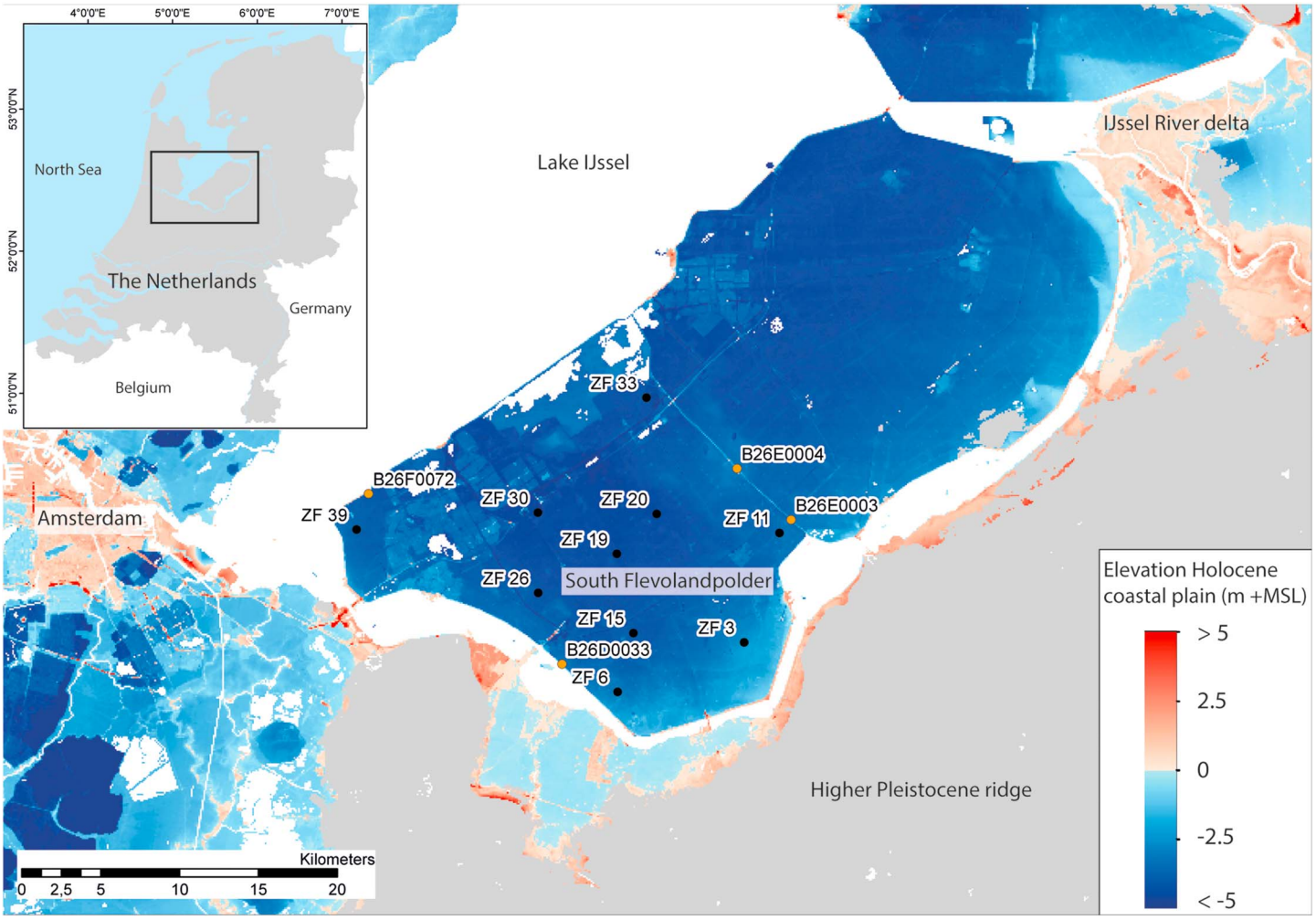

Figure 1. Elevation map of Holocene deposits in the South Flevoland polder and adjacent areas (TNO-GSN, 2016 [TNO, Geological Survey of the Netherlands]), with measurements locations. MSL = mean sea level.

freshwater wetland. Eventually, around 5,000-year BP, the entire area transformed to a freshwater wetland in which vast extended peat layers formed (Vos, 2015). Due to a combination of human and natural causes, the peatlands started to drain around 2,000- to 1,000-year BP, losing vast quantities of volumes, and they eventually submerged (Van den Biggelaar et al., 2014). Parallel to this event, the IJssel river started to debouch in the degrading wetland, forming a delta. From 1,000-year BP onward, the submerged area was subsequently invaded by storm induced sea ingressions, transforming the area into a large inland sea, eroding and covering the peat with clay and sand (Van den Biggelaar et al., 2014).

During historic times, the inland sea flooded the surrounding lands frequently. Therefore, the inland sea was dammed off and became a lake in 1932. Several parts of this lake were reclaimed, of which the South Flevoland polder was the last. Since subsidence after reclamation was expected (De Glopper, 1969), annual surface elevation measurement campaigns were conducted to monitor subsidence (De Glopper, 1984).

3. Materials and Methods

The procedure that we employ to achieve a better understanding and parametrization of the processes that cause subsidence contains three main elements: (1) the available data, (2) a physical description of the processes involved, and (3) a data assimilation procedure to combine those two and to obtain improved parameters. These main elements are detailed in the current section.

Table 1
Categorization of Lithostratigraphic Entities and Their Estimated Properties Used in This Study

Lithology	Bulk density ρ_s (kg/m^3)	Porosity ϕ (−)
Sand	2,000	0.35
Clay	1,400	0.75
Organic clay	1,300	0.80
Peat	1,100	0.85

3.1. Available Data

3.1.1. Land Surface Elevation Measurements

We used surface elevation measurements from 10 locations throughout the South Flevoland polder. These 10 locations were selected because detailed information on the lithological composition and thickness of the different layers of the coastal sequence at present and prior to reclamation is available there (De Lange et al., 2012). The locations are situated in agricultural areas, and the coastal deposits have a current thickness ranging between 1 and 8 m.

Changes in surface levels at the selected locations were determined annually between 1967 and 1993 by geodetic levelling (De Glopper, 1984; Van Dooremolen et al., 1996). The standard deviation of the measurements was estimated to be 0.03 m. The measurements revealed that most subsidence occurred in the first decade after reclamation (average c. 0.06 m/year) and decreased during subsequent decades (average c. 0.02 m/year).

In 2009, a nationwide airborne Lidar surface elevation campaign was performed. Furthermore, surface levels were measured in 2012 prior to investigating the lithological composition of the 10 selected areas. Both measurement series were added to the data set and revealed subsidence rates less than 0.01 m/year between 1993 and 2012. The standard deviations of the Lidar and the GPS measurements were also taken to be 0.03 m.

3.1.2. Lithological Analysis

Prior to reclamation, the subsurface of the South Flevoland polder was investigated by corings. These corings provide information on the initial thickness and lithological composition of the subsurface prior to reclamation and drainage of the area. In 2012, additional series of cored boreholes were analyzed to determine the thickness and composition of the coastal deposits. This yielded insight in changes in subsurface composition and layer thickness after almost half a century of phreatic groundwater level lowering and subsequent subsidence (De Lange et al., 2012). During both coring campaigns, the sediments encountered in the cored boreholes were classified into four different lithologies: sand, clay, organic clay, and peat. For the bulk density and porosity of these lithological classes, typical values of sand and clay encountered in Flevoland (De Glopper, 1989) and peat in the Netherlands were used (Koster, De Lange, et al., 2018; Table 1). Areas with the thickest coastal sequence (4–10 m), that is, the western part of the study area, experienced most subsidence. There, in 1993, the measured subsidence was between 1 and 1.5 m. In areas with a less thick Holocene sequence (<4 m), subsidence was between 0.25 and 1 m. Layers embedded within the underlying Pleistocene sequence have not experienced significant compression: the measurements made in corings prior to reclamation and in 2012 show that the top of the underlying Pleistocene deposits had remained at the same level.

3.1.3. Groundwater Level Measurements

The main driving force for subsidence in the study area has been the drop in phreatic groundwater levels between 1967 (the year prior to reclamation) and 2012. Groundwater level measurements were available on a number of locations (TNO-GSN, 2016). Only few locations with a shallow filter that monitors phreatic groundwater levels were available, however. Therefore, we also used locations with relatively deep filters, under the assumption that the temporal development of the measured levels would be representative for the phreatic groundwater levels (Hopman et al., 2013). Because of the indicative nature of these numbers, however, the groundwater levels and the rate of groundwater level lowering were kept as uncertain numbers; their estimation is a central part of the present work. Clearly, after the estimation has been performed, a check is required on the agreement between these results and the global prior numbers.

The locations of the wells that were used are shown in Figure 1, and a selection of groundwater level measurements is shown in Figure 2. The groundwater levels have been measured in the selected wells prior to or since reclamation of the South Flevoland polder. They typically show a decrease of 1–2 m in the first 10 years after reclamation, after which the levels more or less stabilize. Assuming hydraulic communication between the shallowest measured groundwater heads and the phreatic levels, the development of these heads is an indication of the development of the phreatic levels. Indications of phreatic groundwater levels were also

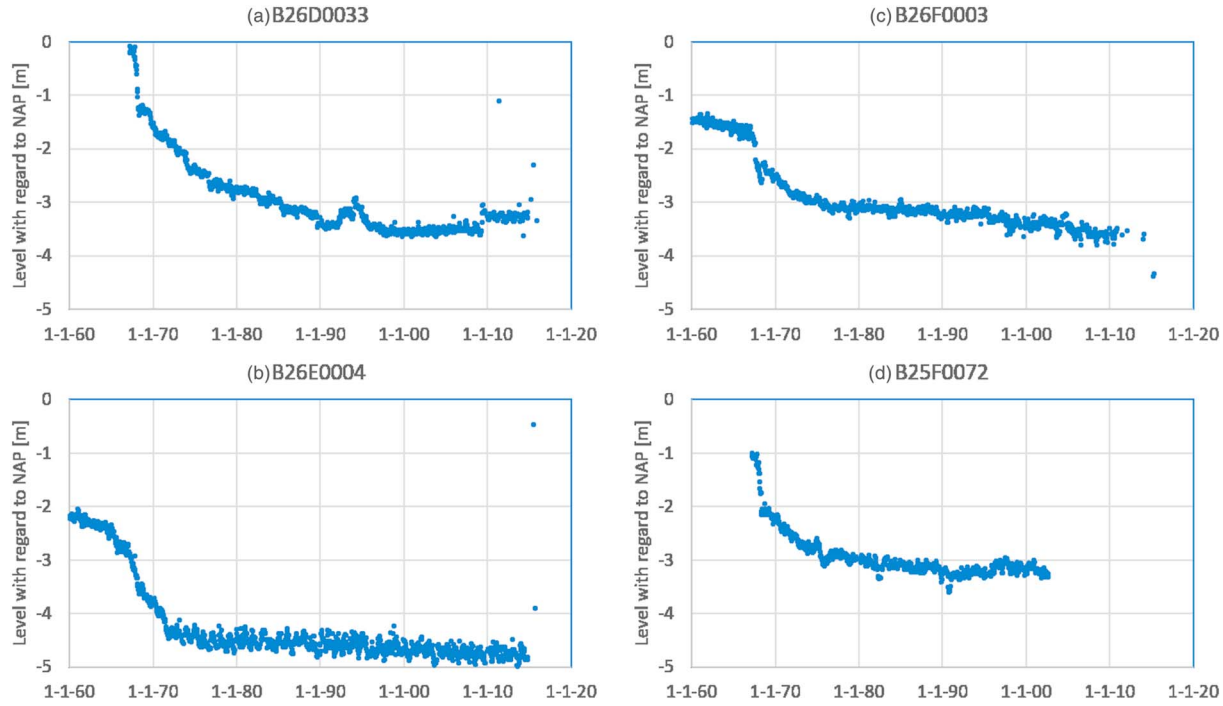

Figure 2. Groundwater levels with regard to NAP, as measured in four different wells (for locations see Figure 1). NAP, the Amsterdam Ordnance Datum, is the official Netherlands height datum and approximates mean sea level. (a) B26D0033, Neighborhoods ZF06, ZF15, and ZF26. Hydraulic head measured at a depth of 6.25–7.25 m below NAP. (b) B26E0003, Neighborhood ZF11. Hydraulic head measured at a depth of 32.0–33.0 m below NAP. (c) B26E0004, Neighborhoods ZF13, ZF20, and ZF33. Hydraulic head measured at a depth of 31.6–32.6 m below NAP. (d) B25F0072, Neighborhood ZF 39. Hydraulic head measured at a depth of 22.4–23.4 m below NAP.

available from the study by De Lange et al. (2012). They show lowest phreatic groundwater levels typically between 1 and 1.50 m below the surface.

3.2. Forward Modelling

We wish to identify the contribution of the different processes and to estimate the parameters that control subsidence, using a data assimilation approach. The processes that control subsidence are schematized in so-called forward models; they represent the underlying physics. How the forward models were deployed in the data assimilation approach for parameter estimation is the subject of the next section.

Prior to reclamation, the area was characterized by coastal marshes, lagoons, and tidal basins, in which layers of subaqueous clay and sand were deposited and peat was formed. The main process in reclamation (after pumping the excess water out of the area) is the artificial lowering of phreatic (ground) water levels to make the area accessible for further land improvements. This human-induced lowering of the phreatic groundwater level is the main driver of subsidence in these areas. It decreases the hydrostatic pressure and, consequently, leads to increased vertical effective stresses, which causes clay and peat layers to compress. Further, clay layers that are situated above the lowered phreatic groundwater level are experiencing negative pore water pressures as a result of evapotranspiration. This increases vertical effective stress and leads to shrinkage as clay particles contract. And finally, aeration of peat layers situated above the lowered phreatic groundwater level results in oxidation of organic matter and subsequently to the disappearance of peat.

We have used generally applied compression and oxidation functions as forward models and added shrinkage to it as an additional mechanism for newly reclaimed land. The total subsidence at the surface level was calculated as the superposition of the compression due to these mechanisms in the affected layers. For compression, two widely applied forward models have been used: the “Koppejan” model and the “NEN-Bjerrum” model (CUR, Centre for Civil Engineering, 1996). Both models depend on effective stresses exerted on the sediments situated above and below the phreatic groundwater level and increases herein when water

levels are lowered. An alternative model that is widely applied in the Netherlands, the a/b/c Isotache model, uses a rate type formulation like the NEN-Bjerrum model but it is based on natural strain rather than linear strain (Den Haan, January 1996; Visschedijk & Trompille, 2009). For the small compression strains that we encountered, the a/b/c Isotache model is equivalent to the NEN-Bjerrum model; we have therefore not used it.

3.2.1. Development of Groundwater Levels and the Associated Effective Stresses

We deployed a two-parameter model to describe the development of phreatic groundwater levels in time for every coring location. This two-parameter model is based on typical groundwater level developments as shown in Figure 2 and on the usual water management strategy for regulating phreatic ground water levels through drainage: The phreatic groundwater level starts decreasing linearly, up to the moment that the final level is reached. From that moment, a fixed value below the surface level is used. The groundwater levels in our modelling are calculated with respect to the surface.

Subsidence is calculated from the combined effects of compression, oxidation, and shrinkage of every individual layer encountered at each of the 10 selected locations. This calculation requires input of the history of the layer, the effective stress and the saturation. We assume layers situated below the phreatic groundwater level to be fully saturated with water (wet layers) and layers above this level to be disposed of all free water (dry layers). We assume that a gradual transition from wet to dry circumstances can be modeled by an abrupt transition—especially since the depth of this transition is an adjustable parameter.

The total vertical stress σ_t in the subsurface equals the overburden weight per unit area. For a layer i with thickness δh_i, total stress increases from top to bottom with

$$\Delta\sigma_{t,i,\mathrm{wet}} = \left[(1-\phi)\rho_{s,i} + \phi\rho_l\right] g\delta h_i \quad \Delta\sigma_{t,i,\mathrm{dry}} = (1-\phi)\rho_{s,i} g\delta h_i \tag{1}$$

With ϕ the soil porosity, $\rho_{s,i}$ the soil grain density of layer i, ρ_l the water density, and g gravitational acceleration constant (Table 1).

The vertical effective stress σ' is the difference between the total stress and the water pressure, and the contribution of each layer is therefore given by

$$\Delta\sigma'_{i,\mathrm{wet}} = \Delta\sigma_{t,i,\mathrm{wet}} - \rho_l \delta h_i = (1-\phi)\left(\rho_{s,i} - \rho_l\right) g\delta h_i \quad \Delta\sigma'_{i,\mathrm{dry}} = \Delta\sigma_{t,i,\mathrm{dry}} = (1-\phi)\rho_{s,i} g\delta h_i \tag{2}$$

The total effective stress in layer n is the superposition of contributions of all layers i above a certain depth:

$$\sigma' = \sum_{i=1}^{n} \Delta\sigma' \tag{3}$$

As a result of the changing elevation in time of the phreatic groundwater level, the transition from wet to dry layers also changes with time. In addition, the compression, shrinkage, and oxidation change the thicknesses of the various layers. These dynamics necessitate a new calculation of the contributions to the effective stress after every time step.

3.2.2. The Koppejan Compression Model

The Koppejan model distinguishes compression by primary consolidation and creep. The model assumes that consolidation under drained conditions occurs instantaneously and that creep is the result of superposition of separate contributions from loading and unloading steps.

Furthermore, the Koppejan model distinguishes between vertical effective stresses smaller (reversible compression) or larger (irreversible compression) than the preconsolidation stress. The preconsolidation stress is the maximum vertical effective stress experienced in the past. At stresses smaller than the preconsolidation stress, the Koppejan model for the thickness change Δh relative to the original thickness h_0 reads

$$\frac{\Delta h}{h_0} = \frac{1}{h_0}\left(\Delta h_{\mathrm{prim}} + \Delta h_{\mathrm{sec}}\right) = \left[\frac{1}{C_p} + \frac{1}{C_s}\log\left(1 + \frac{t}{\tau_0}\right)\right] \ln\left(\frac{\sigma'}{\sigma'_0}\right) \tag{4}$$

Δh_{prim} and Δh_{sec} are the contributions of primary consolidation and creep to the total thickness change; c; τ_0 is a reference time (1 day); t is the time since application of the new effective stress σ', and σ'_0 is the initial

effective stress. At stresses larger than the preconsolidation stress, indicated by σ_p, the Koppejan relationship reads

$$\frac{\Delta h}{h_0} = \frac{1}{h_0}\left(\Delta h_{\text{prim}} + \Delta h_{\text{sec}}\right) = \left[\frac{1}{C_p} + \frac{1}{C_s}\log\left(1+\frac{t}{\tau_0}\right)\right]\ln\left(\frac{\sigma_p}{\sigma_0'}\right) + \left[\frac{1}{C_p'} + \frac{1}{C_s'}\log\left(1+\frac{t}{\tau_0}\right)\right]\ln\left(\frac{\sigma'}{\sigma_p}\right) \quad (5)$$

C_p and C_s are the Koppejan consolidation parameters for the part of the stress that is smaller than the preconsolidation stress; C_p' and C_s' are the Koppejan consolidation parameters for the part of the stress that is larger than the preconsolidation stress.

In the present study, we do not consider swelling. Furthermore, the preconsolidation stress here is the stress at reclamation and equals the initial vertical effective stress; $\sigma_p = \sigma_0'$:

$$\frac{\Delta h}{h_0} = \frac{1}{h_0}\left(\Delta h_{\text{prim}} + \Delta h_{\text{sec}}\right) = \left[\frac{1}{C_p'} + \frac{1}{C_s'}\log\left(1+\frac{t}{\tau_0}\right)\right]\ln\left(\frac{\sigma'}{\sigma_0'}\right) \quad (6)$$

After changes of vertical effective stresses σ', the new stresses are considered as if they had been applied from the start: the time t continues from the time before the change, without any adjustment.

3.2.3. The NEN-Bjerrum Compression Model

The NEN-Bjerrum model is a compression model suitable for determining subsidence in scenarios with loading and unloading the subsurface (Den Haan, January 1996; Visschedijk & Trompille, 2009). It employs a rate-type visco-plastic isotache formulation. The NEN-Bjerrum model is based on linear strain. It has an assumedly more realistic stress dependence of the creep than the Koppejan model and a better description of unloading and reloading (Den Haan, January 1996).

For idealized drained behavior, the NEN-Bjerrum model considers a vertical effective stress σ' that is larger than the original vertical effective stress σ'_0 to cause compression by three mechanisms:

1. the elastic, reversible contribution of a stress smaller than the preconsolidation stress σ_p, which is proportional to $RR\log\frac{\sigma'}{\sigma_0}$, with RR the recompression ratio,
2. primary irreversible consolidation at stresses larger than the preconsolidation stress, proportional to $RR\log\frac{\sigma_p}{\sigma_0} + CR\log\frac{\sigma'}{\sigma_p}$, in which $\sigma_0 < \sigma_p < \sigma'$, and CR is the compression ratio, and
3. secondary consolidation or creep is proportional to $C_\alpha\log\frac{t}{\tau_0}$, with C_α the coefficient of secondary compression and τ_0 the reference time (1 day).

For changing vertical effective stress, these contributions are combined as (Bakr, 2015; Den Haan, January 1996; Visschedijk & Trompille, 2009):

$$\frac{\Delta h}{h_0} = RR\log\frac{\sigma'}{\sigma_0} + C_\alpha\log\left\{1 + \int_0^t\left(\frac{\sigma'}{\sigma_p}\right)^{\frac{CR-RR}{C_\alpha}}\frac{d\tau}{\tau_0}\right\} \quad (7)$$

In this study, the vertical effective stress is only increasing with time, and the preconsolidation stress equals the original stress; $\sigma_0 = \sigma_p$. Stepwise increases in stress can subsequently worked out as (Den Haan, January 1996; Visschedijk & Trompille, 2009):

$$\frac{\Delta h(t)}{h_0} = CR\log\frac{\sigma_n'}{\sigma_0'} + C_\alpha\log\frac{t - t_n + \theta_{n-1}}{\tau_0} \quad (8)$$

$$\theta_n = \left(\frac{\sigma_n'}{\sigma_{n+1}'}\right)^{\frac{CR-RR}{C_\alpha}} \times (\theta_{n-1} + t_n - t_{n-1})$$

$$\theta_0 = \tau_0\left(\frac{\sigma_0'}{\sigma_1}\right)^{\frac{CR-RR}{C_\alpha}}$$

The newly introduced parameters σ_n' and t_n are the vertical effective stress and the time at timestep n (indicated by the subscript), and θ_n is a correction term for the time to account for the stress history and ensure a

smooth transition between subsequent timesteps. Here no compression below the preconsolidation stress was observed. Consequently, the parameter *RR* could not be determined from the data, and therefore, standard documented values for the Netherlands were used (CUR, Centre for Civil Engineering, 1996). The influence of *RR* is limited.

3.2.4. Oxidation Model

Studies conducted in the Netherlands that focused on peat oxidation generally use a fixed annual oxidation rate with respect to the actual thickness of a layer (Koster, Stafleu, & Stouthamer, 2018; Van der Meulen et al., 2007; Van Hardeveld et al., 2017). Because only the organic matter oxidizes, a residual thickness representing admixed clastic sediments should ideally be taken into account. We have implemented this in our models as a fraction of the original thickness, and we denote this fraction as λ_r. If a layer is completely composed of organic matter, the fraction λ_r is 0.

To calculate the thickness reduction of a dry layer during a time step Δt, the part h_{ox} of the layer that is susceptible to oxidation is first determined. This starts with $h_{ox}(t=0) = (1-\lambda_{r,ox})h_o = h_o - \lambda_{r,ox}h_o$ in which h_o is the starting thickness. When part of the layer has already been oxidized, then $h_{ox}(t) = h(t) - \lambda_{r,ox}h_o$. With an oxidation rate V_{ox}:

$$\frac{dh_{ox}}{dt} = -V_{ox}h_{ox} \tag{9}$$

During a time Δt, the reduction of the layer thickness is expressed as follows:

$$\Delta h_{ox} = h_{ox}(t) - h_{ox}(t+\Delta t) = \left(1-e^{-V_{ox}\Delta t}\right)\cdot h_{ox}(t) = \left(1-e^{-V_{ox}\Delta t}\right)\cdot\left(h(t)-\lambda_{r,ox}h_o\right)$$

If the phreatic water level is situated within a peat layer, only the aerated part of the peat layer is oxidizing. Both the total thickness and the part that is precluded from oxidation must be corrected for the wet part:

$$\Delta h_{ox} = \left(1-e^{-V_{ox}\Delta t}\right)\left(h(t)-h_{wet}-\lambda_{r,ox}[h_o-h_{\mathrm{wet}}]\right) \tag{10}$$

3.2.5. Shrinkage Model

Shrinkage of subaqueous deposits is a faster subsidence process than compression and oxidation (Schothorst, 1982). For the South Flevoland Polder, De Glopper (1969) provided a relationship between expected shrinkage of subaqueous deposits and composition (in particular, the specific volume), based on 256 sediment samples. Furthermore, De Glopper (1969) found that increasing clay mineral content relates to increasing shrinkage. However, we have very limited data regarding the composition of South Flevoland Polder clay layers at our measured locations, and we want to arrive at global parameter values. More importantly, De Glopper (1969) (and updates: De Glopper, 1973, 1984, 1989) does not provide an evolution function that can be used to follow shrinkage in time. He only discusses final values after unknown periods of shrinkage. Therefore, we have chosen to implement a simple relationship based on the first-order approximation that the shrinkage rate is proportional to the exposed volume susceptible to it. This is very similar to the degradation of organic matter during oxidation; therefore, we have implemented a relationship similar to the oxidation function that was detailed in the previous paragraph. Indeed, the process is limited by a maximum value beyond which no more shrinkage will occur; and the rate decreases when the accumulated shrinkage reaches this value. With these assumptions we arrive at a shrinkage rate similar to equation (9) and consequently an exponential decay to an equilibrium value like equation (10):

$$\Delta h_{sh} = \left(1-e^{-V_{sh}\Delta t}\right)\left(h-h_{wet}-\lambda_{r,sh}[h_o-h_{\mathrm{wet}}]\right) \tag{11}$$

Analogous to the oxidation, V_{sh} and $\lambda_{r,sh}$ are the shrinkage velocity and the residual thickness fraction. Whether or not this exponential decay is a reasonable assumption must become clear with the results of the study. Another point of discussion is the abrupt division between dry and wet parts of the subsurface. We have assumed that the adjustability of the transition depth should compensate the possible effect of a gradual transition.

3.3. Parameter Estimation Technique

Parameter estimation is possible in many different ways (e.g., Evensen, 2009; Menke, 2012; Tarantola, 2005). The current study, however, is not about selecting an appropriate method for data assimilation but about

evaluating the measurements and scrutinizing between different mechanisms. We have therefore used an established ensemble technique that is appropriate for the current study: Ensemble Smoothing with Data Assimilation, ES-MDA (Emerick & Reynolds, 2013a). This approach is flexible to set up and relatively fast in execution (e.g., Emerick & Reynolds, 2013b). The Ensemble Smoother is appropriate because all measurements are available during the study (there is no progressive addition of measurements during the study), and Multiple Data Assimilation is the appropriate choice to handle the strong nonlinearities in the model. We summarize the main characteristics of the technique in order to give the reader the necessary background. An earlier account of the method, targeted at the assimilation of driving parameters in gas production-induced subsidence, can be found in Fokker et al. (2016).

ES-MDA uses a parameterized description of the subsurface, with an a priori estimation of the parameters, in conjunction with observed data. A forward model calculates subsidence, and the ES-MDA algorithm estimates the parameters by minimizing the mismatch between measured data and estimated values from the model.

The adjustable model parameters and uncertain operational parameters are collected in a vector $\mathbf{m}$. Data are collected in a vector $\mathbf{d}$. The forward model is indicated by a functional $\mathbf{G}(\mathbf{m})$, operating on the parameters. This functional calculates the subsidence in the 10 locations as a function of time, using the parameters given in $\mathbf{m}$.

The inverse problem is formulated as the task of estimating the vector $\widehat{\mathbf{m}}$ for which $\mathbf{G}(\widehat{\mathbf{m}})$ approaches the data vector $\mathbf{d}$ best. With additional information present in the form of a prior model ($\mathbf{m}_0$) and covariance matrices of the measurements ($\mathbf{C}_d$) and of the prior model ($\mathbf{C}_m$), the conventional least squares solution is obtained by maximizing the objective function J, given by *Tarantola* (2005) (or by minimizing the exponent in the expression, $-\log[J]$)

$$J = \exp\left[-\frac{1}{2}(\mathbf{m}-\mathbf{m}_0)^T\mathbf{C}_m^{-1}(\mathbf{m}-\mathbf{m}_0)-\frac{1}{2}(\mathbf{d}-\mathbf{G}(\mathbf{m}))^T\mathbf{C}_d^{-1}(\mathbf{d}-\mathbf{G}(\mathbf{m}))\right] \tag{12}$$

A model vector ensemble is created of N_e vectors, $\mathbf{M} = (\mathbf{m}_1, \mathbf{m}_2, \ldots \mathbf{m}_{N_e})$, by stochastically generating values in the distributions of the parameters, using their mean and covariance. The difference with the prior mean is defined as $\mathbf{M}' = \mathbf{M} - \mathbf{m}_0$. An ensemble of data realizations is created by adding different random noise vectors to the data, that lie within the uncertainty range of the measurements: $\mathbf{D} = (\mathbf{d}+\epsilon_1, \mathbf{d}+\epsilon_2, \ldots \mathbf{d}+\epsilon_{N_e})$. For the noise, a normal distribution is used with a mean of zero and a standard deviation as given by the uncertainty of the data. This procedure ensures a posterior error covariance that is consistent with the theory in the case with Gaussian error statistics (Evensen, 2009). A global update of the model using all available data can be achieved by an Ensemble Smoother (Emerick & Reynolds, 2013b).

To extend Tarantola's solution of a linear inverse problem to an ensemble-based estimate for a nonlinear problem (equation (3.37) from Tarantola, 2005), $\mathbf{GM}$ is defined as the result of the forward model operating on all the members of the model ensemble, replacing his $\mathbf{Gm}$ in which $\mathbf{G}$ is a matrix operating on $\mathbf{m}$. $\mathbf{GM}$ can be visualized as a number of time series (an ensemble) of surface levels versus time. $\mathbf{GM}'$ is defined as the difference between $\mathbf{GM}$ and its average. The model covariance for the ensemble is given by $\mathbf{C}_m = \mathbf{M}'\mathbf{M}'^T/(N_e-1)$. The ensemble smoother then gives as updated model ensemble:

$$\begin{aligned}\widehat{\mathbf{M}} &= \mathbf{M} + \mathbf{M}'\left[\mathbf{GM}'\right]^T\left\{\mathbf{GM}'\left[\mathbf{GM}'\right]^T + (N_e-1)\mathbf{C}_d\right\}^{-1}(\mathbf{D}-\mathbf{GM}) \\ &= \mathbf{M} + \mathbf{M}'\left\{\left[\mathbf{GM}'\right]^T\mathbf{C}_d^{-1}\mathbf{GM}' + (N_e-1)\mathbf{I}\right\}^{-1}\left[\mathbf{GM}'\right]^T\mathbf{C}_d^{-1}(\mathbf{D}-\mathbf{GM})\end{aligned} \tag{13}$$

The two expressions are equivalent and one of them can be chosen according to the smallest required computing time. The new estimate is $\widehat{\mathbf{m}}=\widehat{\mathbf{M}}$, averaged over all the ensemble members, and the posterior covariance is $\mathbf{C}_{\widehat{\mathbf{m}}}=\widehat{\mathbf{M}}'\widehat{\mathbf{M}}'^T/(N_e-1)$. The posterior covariance of the data forecasts is given by $\mathbf{C}_{\widehat{\mathbf{gm}}}=\widehat{\mathbf{GM}}'\widehat{\mathbf{GM}}'^T/(N_e-1)$

For linear problems, the ensemble smoother is equivalent to linear inversion if the ensemble is large enough. However, the estimate is suboptimal when the forward model contains nonlinearities. After

evaluating several possible approaches, Emerick and Reynolds (2013a) and Tavakoli et al. (2013) concluded that the best approach for nonlinear systems where all data can be used simultaneously is to use the ES-MDA. In ES-MDA, an ensemble smoother is applied multiple times. The output ensemble of the smoother is sequentially used as input ensemble for the next update, with the same data. This procedure is repeated a number of times. In this way, correlations between parameters that result from the smoother are retained in subsequent steps. To compensate for the effect of the multiple application, the data covariances used in the update steps are increased with respect to the actual covariance. The covariance multiplication factors α_i must be chosen so that $\sum_{i=1}^{N_a} \frac{1}{\alpha_i} = 1$ (with N_a the number of assimilation steps). We used eight steps with α_i decreasing from 50 to 2.9 with increasing i, giving progressively larger weight to later update steps. In total, 200 realizations as ensemble members were used. Both the number of steps and the number of ensemble members were found after sensitivity runs with varying numbers, as an optimum between minimizing both the computing time and the improvement achieved with larger numbers.

A quality estimate of the assimilation result can be provided when the covariance of both the data and the forecasts with the estimated parameters are known. The test function is constructed as follows:

$$\chi^2 = \left(\widehat{\mathbf{GM}}-\mathbf{d}\right)^{\boldsymbol{T}} \left(\mathbf{C}_d + \mathbf{C}_{\widehat{\mathbf{gm}}}\right)^{-\mathbf{1}} \left(\widehat{\mathbf{GM}}-\mathbf{d}\right) \tag{14}$$

This function should adhere to a χ^2 distribution—that is, the expected value is the degree of freedom, N_d. The scaled parameter χ^2/N_d should be about unity.

4. Results

The parameters that were estimated are the following:

1. six model parameters for compression (primary consolidation and creep parameters for both the Koppejan and the NEN-Bjerrum model; independent sets of two parameters for clay, for organic clay, and for peat—making six parameters),
2. model parameters for oxidation (oxidation velocity and relative residual thickness of peat),
3. model parameters for shrinkage (shrinkage rate and relative residual thickness of clay and of organic clay), and
4. the 20 operational parameters for the groundwater development (for each of the 10 locations the initial groundwater lowering rate and the final level).

These numbers accumulate to a total of 32 adjustable parameters.

The results for the simultaneous assimilation of all-time series and parameters to the data are represented in Figure 3, for both the NEN-Bjerrum and the Koppejan model. Measurements are indicated as symbols. The time series calculated with the prior ensemble are not indicated in the figure—they are vastly varying. Most of them do not follow the measurements, but the measurements are located within the bandwidth of the calculations.

The time series in Figure 3 represent the 200 modelled surface movement developments for the ensemble of assimilated parameters. The prior and estimated parameters are given in Table 2. The models follow the measurements well, which is in accordance with the quality values (χ^2/N_d) for the two models of 1.56 and 1.75, respectively. The deviation from unity can be easily understood from a slight underestimation of the data uncertainty. If the actual uncertainty is 30% larger than assumed in the assimilation exercise, the quality measure would drop to about unity (because the contribution of Cd in equation (14) would increase by a factor 1.7). The NEN-Bjerrum performs slightly better than the Koppejan model; however, the small difference in quality is not decisive for choosing either one. The spread of the time series, visualized by the expanding wake of forecasts in the figure, is of the same order of magnitude as the uncertainty of the measurements, demonstrating the proper action of the Smoother and the circumvention of ensemble collapse.

In Figure 4, the thickness and lithological composition of the subsurface layers measured in 1967 and 2012 and the calculated thickness of the layers from the model estimates in 2012 are presented. The 2012 forecast

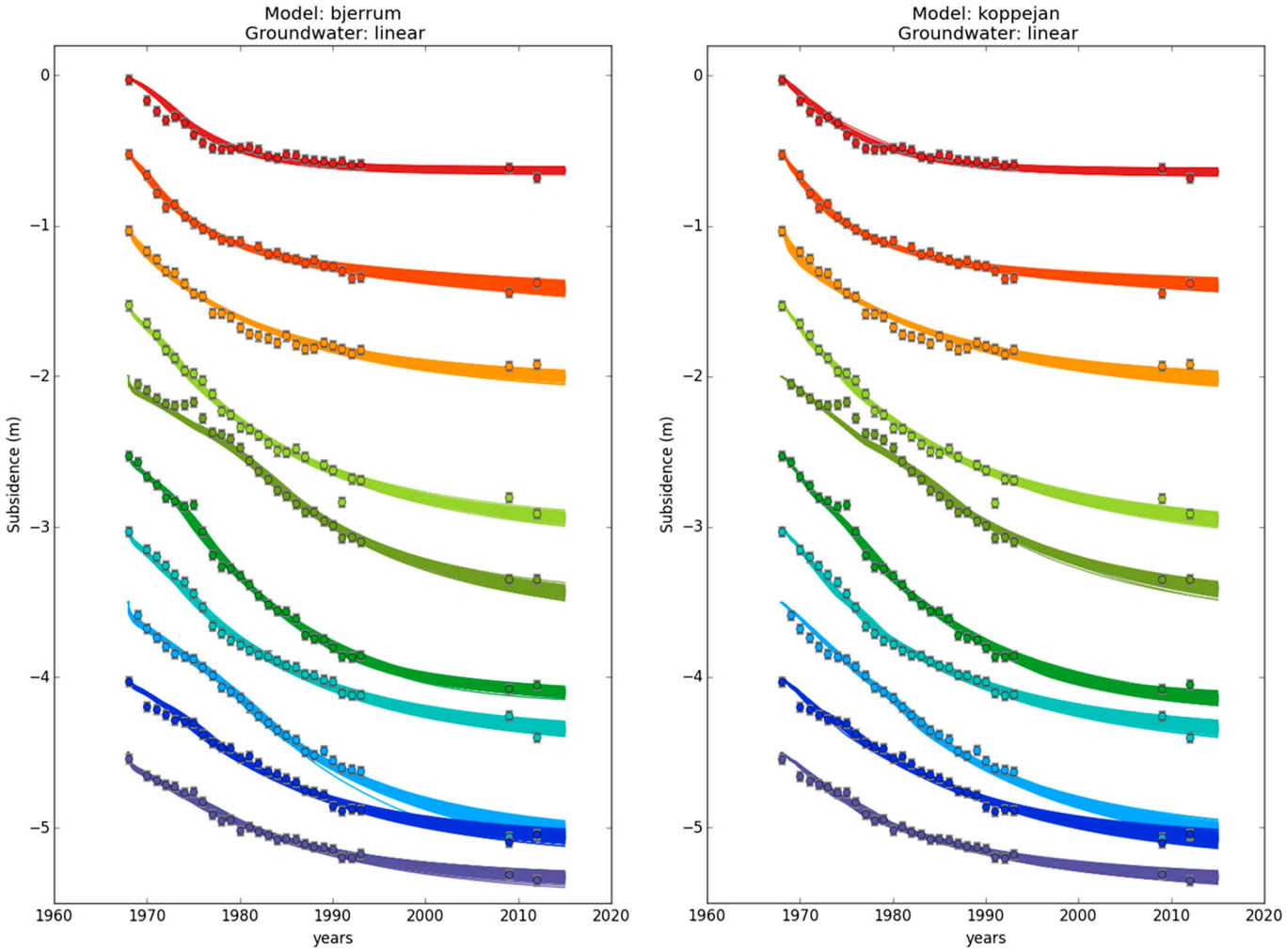

Figure 3. Time series of all surface subsidence development matched simultaneously for the NEN-Bjerrum model (left) and the NEN-Koppejan model (right), combined with oxidation and shrinkage. Time series of subsequent locations are translated 0.5 m vertically for clarity. Symbols indicate the measurements and their standard deviation. Lines represent the 200 realizations of the models for the ensemble of estimated parameters. From top to bottom, the timeseries indicate all wells ZF03 to ZF39 (listed in Table 2).

of the thicknesses of the layers is in reasonable agreement with the 2012 measurements. The discrepancies that are observed may be related to a different interpretation technique and to slightly different locations, with distances of up to 20 m laterally from the surface subsidence measurement point.

5. Discussion

5.1. Contributing Processes and Associated Parameters

The contribution of different subsidence processes is highlighted in Figure 5, showing that for all the locations shrinkage constitutes the main contribution. The shrinkage parameters, groundwater levels, and decrease rates are comparable for the NEN-Bjerrum and the Koppejan models. For the shrinkage rates, we have no data to compare to, but these rates being larger than the oxidation rates for the peat is in line with qualitative statements found in the literature (Schothorst, 1982). Furthermore, the residual thickness factor that we found (0.67 for clay and 0.47 for organic clay) is in line with the indications of pioneering studies conducted in the South Flevoland Polders (De Glopper, 1969, 1973, 1984, 1989): He indicates values between 0.90 and 0.40 when increasing the clay content from 5% to 60%.

Oxidation was only effective in well ZF06, where peat was seen to be aerated. Primary consolidation and creep was only active shortly after the start of the time series. This is related to the logarithmic

Table 2
Prior and Estimated Parameters for Assimilation of All-Time Series (Number in Brackets Signifies Standard Deviation in Units of the Last Digit(s))

Parameter	NEN-Bjerrum prior	NEN-Bjerrum estimate	Koppejan prior	Koppejan estimate
CR Clay	0.050(20)	0.080(20)		
C_α Clay	0.0100(50)	0.0060(11)		
CR Organic Clay	0.050(20)	0.051(15)		
C_α Organic Clay	0.0100(50)	0.0091(14)		
CR Peat	0.050(20)	0.090(30)		
C_α Peat	0.0100(50)	0.0060(15)		
Cp Clay			10(5)	26(8)
Cs Clay			50(20)	116(30)
Cp Organic Clay			10(5)	15(3)
Cs Organic Clay			50(20)	86(23)
Cp Peat			10(5)	7(2)
Cs Peat			50(20)	65(18)
V_{sh} Clay	0.10(5)	0.27(2)	0.10(5)	0.17(2)
λ_r Clay	0.50(20)	0.67(2)	0.50(20)	0.66(3)
V_{sh} Organic Clay	0.030(15)	0.138(6)	0.030(15)	0.133(9)
λ_r Organic Clay	0.250(100)	0.469(12)	0.250(100)	0.478(15)
V_{ox} peat	0.0100(50)	0.0123(17)	0.0100(50)	0.0088(16)
λ_r peat	0.100(40)	0.090(30)	0.100(40)	0.088(26)
ZF03 gw	1.30(20)	1.44(16)	1.30(20)	1.42(17)
ZF03 gw'	0.20(10)	0.26(3)	0.20(10)	0.35(5)
ZF06 gw	1.90(20)	1.91(15)	1.90(20)	1.97(15)
ZF06 gw'	0.20(10)	0.52(7)	0.20(10)	0.31(4)
ZF11 gw	1.10(20)	1.15(3)	1.10(20)	1.17(3)
ZF11 gw'	0.20(10)	0.75(20)	0.20(10)	0.47(10)
ZF15 gw	1.10(20)	1.54(4)	1.10(20)	1.51(5)
ZF15 gw'	0.20(10)	0.32(3)	0.20(10)	0.181(11)
ZF19 gw	1.10(20)	1.63(4)	1.10(20)	1.54(4)
ZF19 gw'	0.20(10)	0.107(4)	0.20(10)	0.080(3)
ZF20 gw	1.10(20)	1.78(7)	1.10(20)	1.72(7)
ZF20 gw'	0.20(10)	0.232(14)	0.20(10)	0.157(8)
ZF26 gw	1.20(20)	1.58(3)	1.20(20)	1.49(3)
ZF26 gw'	0.20(10)	0.227(18)	0.20(10)	0.145(8)
ZF30 gw	1.20(20)	1.70(4)	1.20(20)	1.63(4)
ZF30 gw'	0.20(10)	0.124(7)	0.20(10)	0.103(5)
ZF33 gw	1.10(20)	1.27(3)	1.10(20)	1.30(4)
ZF33 gw'	0.20(10)	0.170(14)	0.20(10)	0.151(12)
ZF39 gw	1.10(20)	0.93(3)	1.10(20)	0.93(3)
ZF39 gw'	0.20(10)	0.101(10)	0.20(10)	0.095(7)

Note. The upper part of the table contains the material properties (compression, oxidation, and shrinkage). The lower part contains the groundwater level parameters. Each location is associated with a final value (gw, in meters depth relative to surface level of 2012) and a level decrease rate (m/year, gw').

relationships in these processes. Without including shrinkage, it was impossible to arrive at acceptable results, even with parameters that were vastly out of their normal range. An earlier study in which we attempted to fit the data without the incorporation of shrinkage resulted in unphysical values for the adjustable parameters: The values for the NEN-Bjerrum or Koppejan parameters were typically an order of magnitude off, and groundwater levels were typically 1 m too low (Fokker et al., 2015). Still, the matches were unacceptable with quality factors in the order of 60. This is highlighted in Figure 6. The qualitative behavior of the curves, dictated by the logarithmic dependence of the compression models on time, is seen to be completely off the observed behavior. The subsidence in this reclaimed land is apparently primarily controlled by the shrinkage upon dewatering the shallowest layers. Therefore, reintroducing shrinkage in shallow subsidence studies in the Netherlands is of utmost importance.

We evaluated the sensitivity to the different parameters by constructing ensembles in which only a single parameter was varied with respect to the estimated mean. This yielded results in line with the evaluation

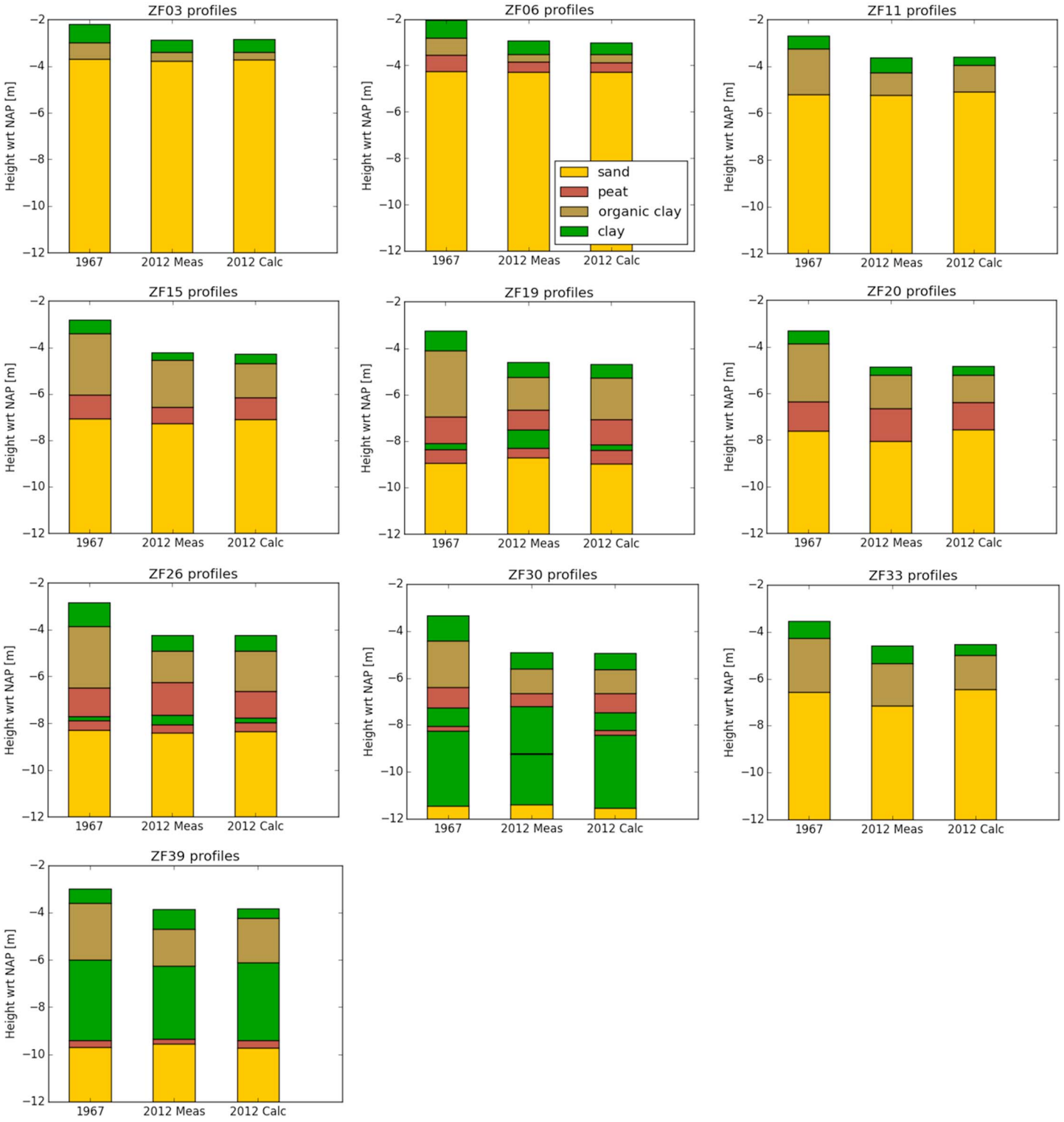

Figure 4. Lithologies for the 10 locations as measured in 1967 and in 2012 and as resulting from the estimates using the NEN-Bjerrum model in 2012. Depth on the *y* axis is relative to Netherlands height datum, NAP (approximate mean sea level)

of different contributions to compression as presented in Figure 5. Highlights are presented in Figure 7. Primary consolidation and creep parameters had minor influence—only the ones for clay had some influence on the time series for ZF30 and ZF39. The shrinkage parameters had a much larger influence.

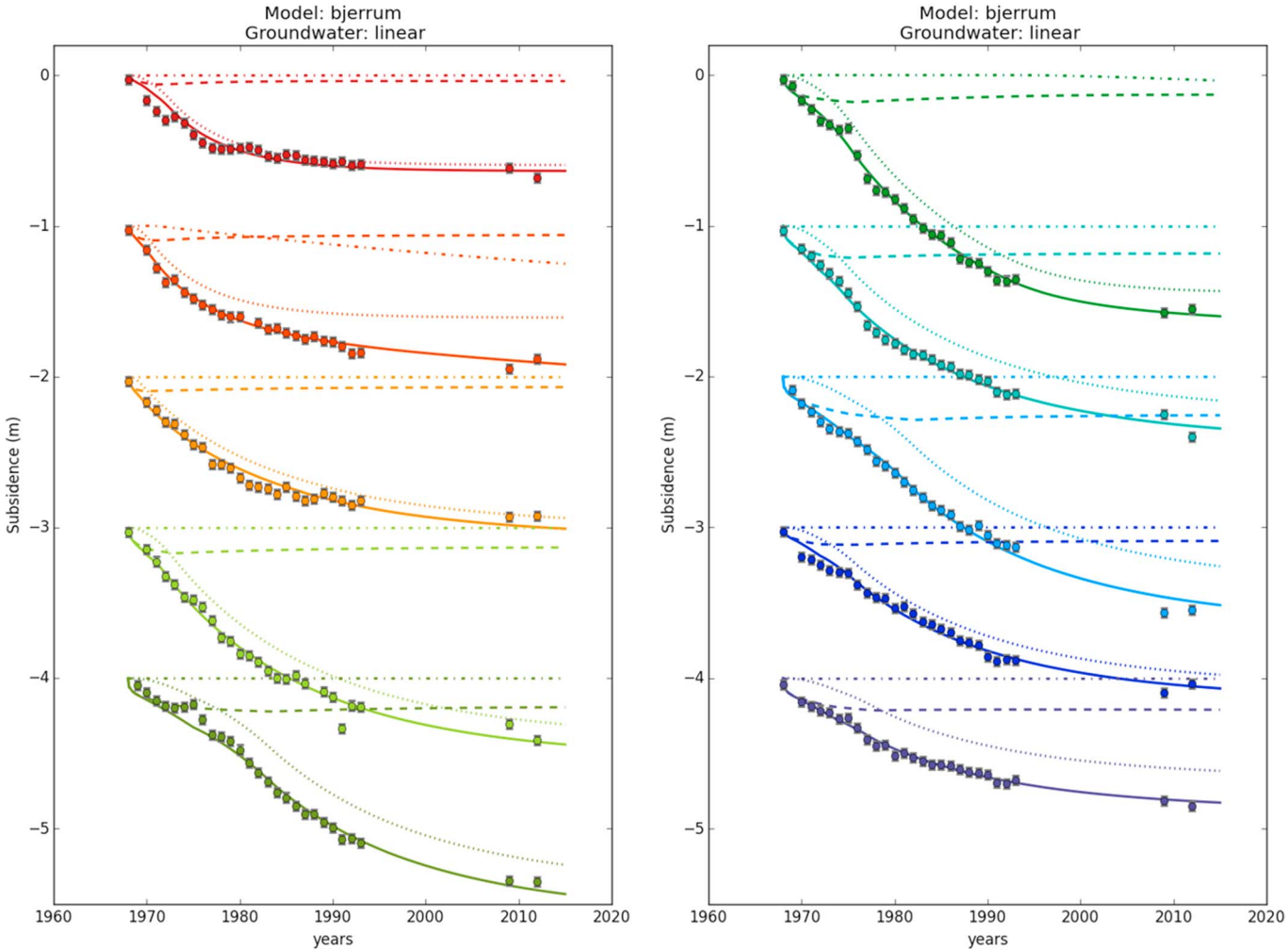

Figure 5. Identification of different contributions to subsidence for the mean case with the NEN-Bjerrum model with linear groundwater level reduction. Dashed lines: primary consolidation and creep; dashed-dotted lines: oxidation; dotted lines: shrinkage; and continuous lines: total. Time series of subsequent locations are translated 1.0 m vertically for clarity. Color codes are identical to the ones in Figure 3.

Varying the shrinkage rate and the residual height for organic clay results in a delay of the variation of subsidence rates because the groundwater level must first pass the top clay layer in all locations. Peat oxidation parameters had minor influence because most of the peat layers remained below the groundwater level for the complete monitoring time. In accordance with Figure 5, only well ZF06 was affected. The groundwater decrease rates and the final groundwater levels have effects as expected: The rate influences the subsidence rate at that particular location until the final value of the groundwater decrease is obtained; it is the ultimate phreatic groundwater level, in combination with the shrinkage parameters, which controls the final amount of subsidence achieved. As an example, the time series for varying the groundwater parameters of ZF20 are shown (Figure 7).

The output ensemble from the Ensemble Smoother also gives possible correlations between the posterior parameter values. Not surprisingly, the largest correlations are between the shrinkage parameters and the water levels and water level reduction rates. A reduction of the shrinkage parameters can be partly compensated by an increase of the dry zone in the various wells. The correlations, however, were not very strong. The poorly constrained parameters, such as the primary consolidation and creep parameters, did not correlate with other parameters. It turned out that the posterior values of the important parameters were well constrained. A poorly constrained inverse problem as is often the case when too many parameters are present or when different parameters are too strongly correlated (Kroon et al., 2009) was not an issue here.

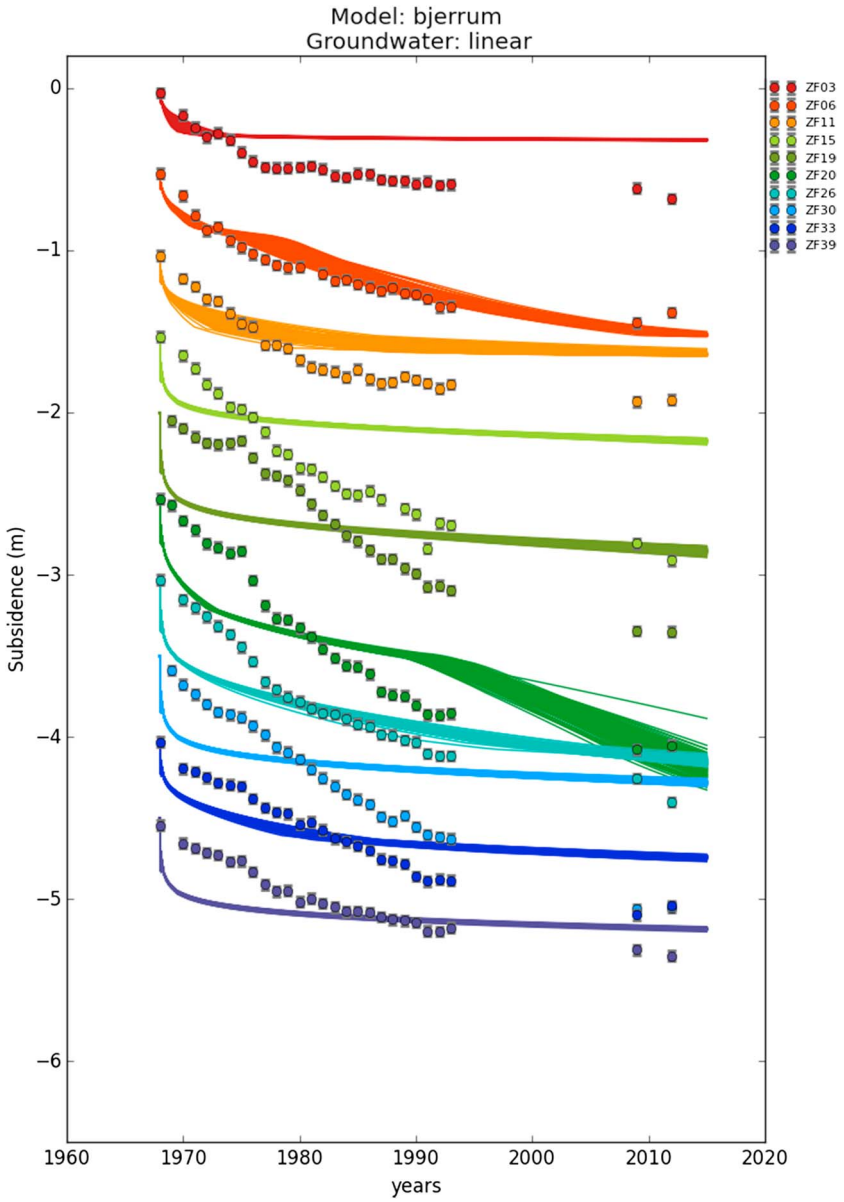

Figure 6. Time series of all surface subsidence development matched simultaneously for the NEN-Bjerrum model; combined with oxidation but without shrinkage. The qualitative response of the surface cannot be reproduced. The reasonable response in ZF06 is related to the aerated peat on that location.

For locations with a thick Holocene sequence on top of the Pleistocene sand layers, like ZF15, ZF19, ZF20, ZF26 and ZF30, the final subsidence is larger than for the other locations. This was expected because of the larger thickness of layers that are compressing. The only exception is ZF39, which is a location with a relatively shallow phreatic groundwater level and hence less forcing to compression.

5.2. Groundwater Levels

The values of average highest, average lowest, and measured groundwater levels as measured by De Lange et al. (2012) for the 10 selected locations are represented in Table 3. They are compared with the estimates resulting from the data assimilation through NEN-Bjerrum and Koppejan (note that both assimilation exercises employ shrinkage of clay and organic clay when they are located above the phreatic level). Estimates in Table 3 are based on multiple estimation exercises with both models and with varying starting values.

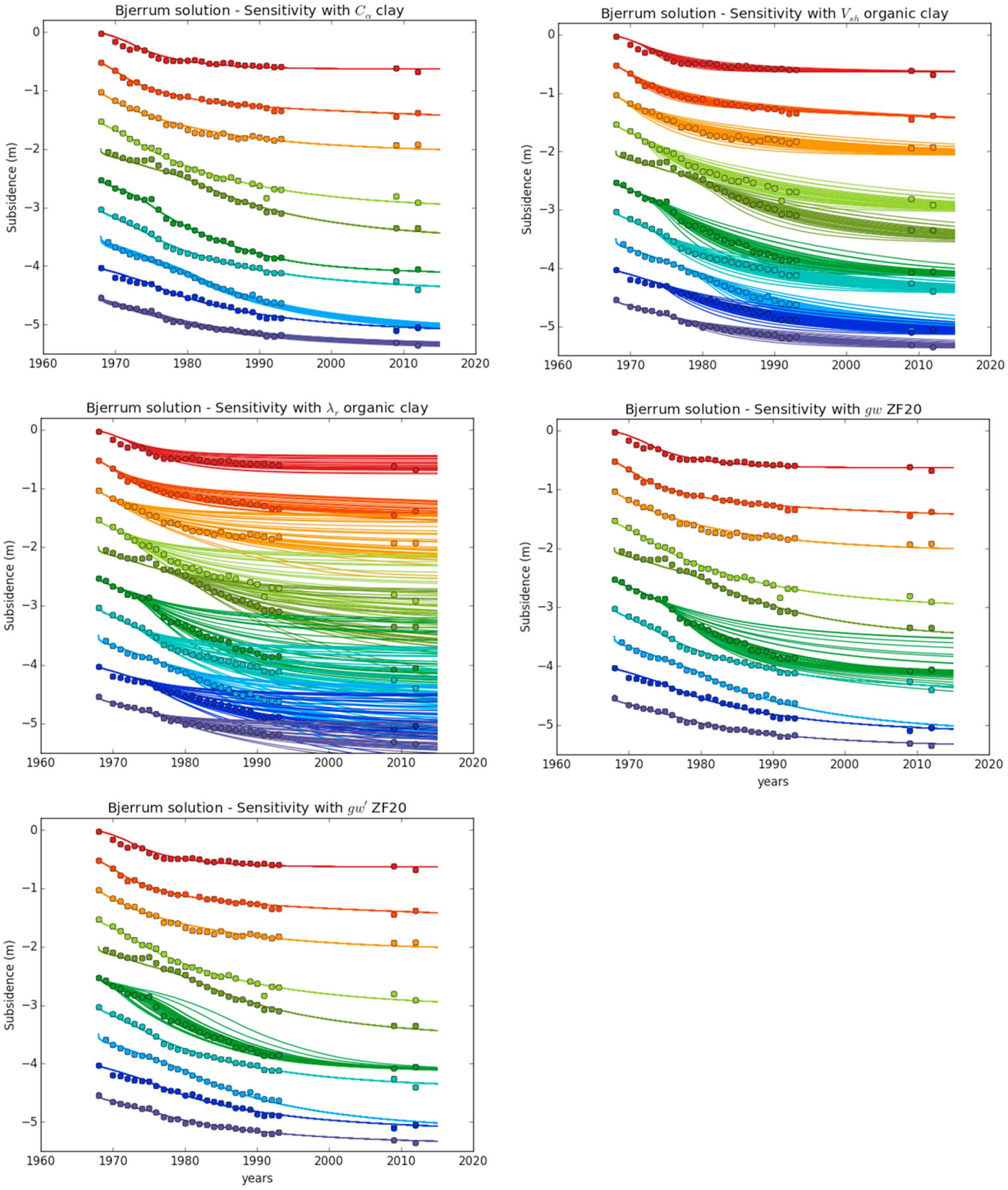

Figure 7. Sensitivity to variation of some selected individual parameters, as indicated by the plot titles: C_α (clay); V_{sh} (organic clay); λ_r (organic clay); gw (ZF20); and gw' (ZF20)

Table 3
Measured Groundwater Levels and Estimated Values From Data Assimilation (in Meter With Respect to the Surface)

Location	Average shallowest	Measured level	Average deepest	Estimate	Estimated rate (m/year)
ZF03	0.50	0.75	1.65	1.3–1.5	0.3–0.4
ZF06	0.70	1.30	1.75	1.8–1.9	0.3–0.4
ZF11	0.50	0.80	1.20	1.1–1.2	0.5–0.7
ZF15	0.60	0.75	1.15	1.5–1.6	0.2–0.3
ZF19	0.50	1.00	1.20	~1.6	0.08–0.10
ZF20	0.50	0.75	0.85	1.7–1.9	0.17–0.20
ZF26	0.60	0.90	1.20	1.4–1.6	0.16–0.20
ZF30	0.50	0.90	1.20	1.6–1.8	0.09–0.12
ZF33	0.45	0.80	1.15	1.2–1.4	0.14–0.17
ZF39	0.50	0.90	1.10	0.8–1.0	0.07–0.11

Note. Estimates in accordance with the measured levels are indicated with green shading. Estimated rates are shaded orange, yellow, and blue for fast, intermediate, and slow values.

The estimated final water levels in ZF03, ZF06, ZF11, ZF33, and ZF39 are in line with the measured ones, while for the other locations the estimated values are too deep. Further, the groundwater decrease rates are relatively fast for the locations ZF03, ZF06, and ZF11, slow for ZF19, ZF30, and ZF39, and moderate for the others. The decrease rates are clearly related to the thickness of the Holocene layers (Figure 4): The low-permeability clay and organic clay layers impede the lowering of the water level. Note that the consolidation because of pressure diffusion is approximated by a linear decrease of the phreatic water level in our approach.

The relationship with the final groundwater levels is more complicated. It seems that the thin Holocene layers allow better estimates than the thicker ones. We think this is related to what the models have been formulated for: they were developed for relatively quick settlement and desettlement of layers. As a consequence, they may perform less for thicker layers. It might be necessary to reassess the logarithmic functional dependencies in both the NEN-Bjerrum and the Koppejan models and the exponential relationship for shrinkage.

The results presented here treat the data as distinct points in space, and they do not consider the regional distribution of geological layers and the associated groundwater dynamics that would require an integrated modelling approach of groundwater dynamics, consolidation and shrinkage, also including all groundwater level measurements. Such a study was beyond the present scope, but we intend to take that up in the near future. Only with such a study, a regional forecast of subsidence will be feasible. An important ingredient of such a study, however, are the model parameters and the understanding of the mechanisms at work that we have proposed in this study.

6. Conclusions

This paper documents an estimation exercise for the parameters driving shallow subsidence in the reclaimed South Flevoland area by compression (i.e., primary consolidation and creep), oxidation, and shrinkage, with the use of historic surface movement data. An exposition of the deliberations leading to the present conclusions is provided in the previous section. The identification of shrinkage as the main contributor to subsidence of the recently reclaimed land is a reintroduced new insight.

It proved to be possible to match the temporal time series of subsidence with the models employed. In particular, the gradual lowering of the groundwater level in the first years after reclamation and the following ongoing shrinkage played a crucial role in explaining the slow start of the subsidence and the acceleration at later times. This is related to the gradual exposure of deeper layers developing negative pore water pressures when exposed to air.

Our analysis shows the importance of having good resolution of data in time and space. The subsurface lithology and the temporal development of the groundwater levels proved to be essential to make good matches. However, the physics of the consolidation model need to be critically reviewed because for

locations with substantial clay and organic clay layers staying below the groundwater level, the estimated groundwater levels were consistently too deep.

A difference between our approach and most other approaches is that we fundamentally include uncertainty estimates or confidence areas. This is facilitated by the ensemble approach that we take. As a consequence, the quality of the model estimates and of the decisions based on it can be assessed with a scientific basis.

Regional estimates can be made when detailed knowledge is available on the regional geology and the history of regional groundwater dynamics.

Acknowledgments
The data used are listed in the references, tables, and supporting information. We thank our reviewers for their useful and constructive comments.

References

Abd El-Kawy, O. R., Rod, J. K., Ismail, H. A., & Suliman, A. S. (2011). Land use and land cover change detection in the western Nile delta of Egypt using remote sensing data. *Applied Geography*, *31*(2), 483–494. https://doi.org/10.1016/j.apgeog.2010.10.012

Auerbach, L. W., Goodbred, S. L. Jr., Mondal, D. R., Wilson, C. A., Ahmed, K. R., Roy, K., et al. (2015). Flood risk of natural and embanked landscapes on the Ganges-Brahmaputra tidal delta plain. *Nature Climate Change*, *5*(2), 153–157. https://doi.org/10.1038/nclimate2472

Bakr, M. (2015). Influence of groundwater management on land subsidence in deltas. *Water Resources Management*, *29*(5), 1541–1555. https://doi.org/10.1007/s11269-014-0893-7

Bronswijk, J. J. B. (1989). Prediction of actual cracking and subsidence in clay soils. *Soil Science*, *148*(2), 87–93. https://doi.org/10.1097/00010694-198908000-00002

Castellazzi, P., Martel, R., Galloway, D. L., Longuevergne, L., & Rivera, A. (2016). Assessing groundwater depletion and dynamics using GRACE and InSAR: Potential and limitations. *Groundwater*, *54*(6), 768–780. https://doi.org/10.1111/gwat.12453

Chena, X., & Zong, Y. (1999). Major impacts of sea-level rise on agriculture in the Yangtze delta around Shanghai. *Applied Geography*, *19*(1), 69–84. https://doi.org/10.1016/s0143-6228(98)00035-6

CUR, Centre for Civil Engineering (1996). *Building on soft soils* (p. 500). London: Routledge.

Day, J. W., Agboola, J., Chen, Z., D'Elia, C., Forbes, D. L., Giosan, L., et al. (2016). Approaches to defining deltaic sustainability in the 21st century. *Estuarine, Coastal and Shelf Science*, *183*, 275–291. https://doi.org/10.1016/j.ecss.2016.06.018

De Glopper, R. J. (1969). *Shrinkage of subaqueous sediments of Lake IJssel (The Netherlands) after reclamation. Proc. First Int. Symp. On Land Subsidence* (pp. 192–201). Tokyo: IAH.

De Glopper, R. J. (1973). Subsidence after drainage of the deposits in the former Zuyder Zee and in the brackish and marine forelands in The Netherlands. Van Zee tot Land 50. (pp. 205).

De Glopper, R. J. (1984). *Subsidence in the recently reclaimed IJsselmeerpolder "Flevoland". Proc. Third Int. Symp. On Land Subsidence* (pp. 487–496). Venice: IAHS.

De Glopper, R. J. (1989). Land subsidence and soil ripening. Rijkswaterstaat, Flevobericht Report 306 (pp. 45).

De Lange, G. Gunnink, J. L., Houthuessen, Y., & Muntjewerff, R. (2012). Bodemdalingskaart Flevoland (Grontmij report).

Den Haan, E. (January 1996). A compression model for non-brittle soft clays and peat. *Géotechnique*, *46*(1), 1–16. https://doi.org/10.1680/geot.1996.46.1.1

Doornkamp, J. C. (1993). Clay shrinkage induced subsidence. *The Geographical Journal*, *159*(2), 196–202. https://doi.org/10.2307/3451410

Drexler, J. Z., De Fontain, C. S., & Deverel, S. J. (2009). The legacy of wetland drainage on the remaining peat in the Sacramento-San Joaquin Delta, California, USA. *Wetlands*, *29*(1), 372–386. https://doi.org/10.1672/08-97.1

Emerick, A., & Reynolds, A. (2013a). Ensemble smoother with multiple data assimilation. *Computer & Geosciences*, *55*, 3–15. https://doi.org/10.1016/j.cageo.2012.03.011

Emerick, A., & Reynolds, A. C. (2013b). Investigation of the sampling performance of ensemble-based methods with a simple reservoir model. *Computer & Geosciences*, *17*, 325–350. https://doi.org/10.1007/s10596-012-9333-z.G.

Evensen, G. (2009). *Data assimilation, The Ensemble Kalman Filter* (2nd ed.). Heidelberg: Springer.

Fokker, P. A., Gunnink, J. L., De Lange, G., Leeuwenburgh, O., & Van der Veer, E. F. (2015). Compaction parameter estimation using surface movement data in Southern Flevoland. *Proceedings of the International Association of Hydrological Sciences*, *372*, 183–187. https://doi.org/10.5194/piahs-372-183-2015

Fokker, P. A., Wassing, B. B. T., Van Leijen, F. J., Hanssen, R. F., & Nieuwland, D. A. (2016). Application of an ensemble smoother with multiple data assimilation to the Bergermeer gas field, using PS-InSAR. *Geomechanics for Energy and the Environment*, *5*, 16–28. https://doi.org/10.1016/j.gete.2015.11.003

Gambolati, G., Putti, M., Teatini, P., & Gasparetto Stori, G. (2006). Subsidence due to peat oxidation and impact on drainage infrastructure in a farmland catchment south of the Venice Lagoon. *Environmental Geology*, *46*, 814–820.

Hopman, V., de Lange, G., Vonhögen, L., Kruiver, P., van Leijen, F., & Ianoschi, R. (2013) Thematic maps Rhine-Meuse Delta, SubCoast report D3.2.2. Retrieved from http://www.subcoast.eu/alfresco/d/d/workspace/SpacesStore/80e6a698-1a23-4b13-b0d0-9a8cbe2d2c8c/D3.2.2 SubCoast thematic maps Rhine Meuse Delta.pdf

Koster, K., De Lange, G., Harting, R., De Heer, E., & Middelkoop, H. (2018). Characterizing void ratio and compressibility of Holocene peat with CPT for assessing coastal-deltaic subsidence. *Quarterly Journal of Engineering Geology and Hydrogeology*, *51*(2), 210–218. https://doi.org/10.1144/qjegh2017-120

Koster, K., Stafleu, J., & Stouthamer, E. (2018). Differential subsidence in the urbanised coastal-deltaic plain of the Netherlands. *Netherlands Journal of Geosciences*, *97*(4), 215–227. https://doi.org/10.1017/njg.2018.11

Kroon, I. C., Nguyen, B. L., Fokker, P. A., Muntendam-Bos, A. G., & de Lange, G. (2009). Disentangling shallow and deep processes causing surface movement. *Mathematical Geosciences*, *41*(5), 571–584. https://doi.org/10.1007/s11004-008-9197-x

Li, L., Zhang, M., & Katzenstein, K. (2017). Calibration of a land subsidence model using InSAR data via the ensemble Kalman filter. *Groundwater*, *55*(6), 871–878. https://doi.org/10.1111/gwat.12535

Menke, W. (2012). *Geophysical data analysis: Discrete inverse theory: MATLAB edition* (Vol. 45). San Diego, CA: Academic press.

Muntendam-Bos, A. G., Kleuskens, M. H. P., Bakr, M., De Lange, G., & Fokker, P. A. (2009). Unraveling shallow causes of subsidence. *Geophysical Research Letters*, *36*, L10403. https://doi.org/10.1029/2009GL037190

Nieuwenhuis, H. S., & Schokking, F. (1997). Land subsidence in drained peat areas of the province of Friesland. *Quarterly Journal of Engineering Geology and Hydrogeology*, *30*(1), 37–48. https://doi.org/10.1144/GSL.QJEGH.1997.030.P1.04

Peduto, D., Huber, M., Speranza, G., van Ruijven, J., & Cascini, L. (2016). DInSAR data assimilation for settlement prediction: Case study of a railway embankment in the Netherlands. *Canadian Geotechnical Journal*, *54*(4), 502–517.

Renaud, F. G., Syvitski, J. M. P., Sebesvari, Z., Werners, S. E., Kremer, H., Kuenzer, C., et al. (2013). Tipping from the Holocene to Anthropocene: How threatened are major world deltas? *Current Opinion in Environmental Sustainability*, *5*(6), 644–654. https://doi.org/10.1016/j.cosust.2013.11.007

Schothorst, C. J. (1977). Subsidence in low moor peat soils in the western Netherlands. *Geoderma*, *17*(4), 265–291. https://doi.org/10.1016/0016-7061(77)90089-1

Schothorst, C. J. (1982). Drainage and behaviour of peat soils. In H. de Bakker & M. W. van den Berg (Eds.), *Proceedings of the symposium on peat lands below sea level* (Vol. 30, pp. 130–163). Wageningen, Netherlands: ILRI-publication.

Tarantola, A. (2005). *Inverse problem theory and methods for model parameter estimation*. Paris, France: SIAM.

Tavakoli, R., Yoon, H., Delshad, M., ElSheikh, A. H., Wheeler, M. F., & Arnold, B. W. (2013). Comparison of ensemble filtering algorithms and null-space Monte Carlo for parameter estimation and uncertainty quantification using CO_2 sequestration data. *Water Resources Research*, *49*, 8108–8127. https://doi.org/10.1002/2013WR013959

Teatini, P., Ferronato, M., Gambolati, G., & Gonella, M. (2006). Groundwater pumping and land subsidence in the Emilia-Romagna coastland, Italy: Modeling the past occurrence and the future trend. *Water Resources Research*, *42*, W01406. https://doi.org/10.1029/2005WR004242

TNO-GSN (2016). Online portal for digital geo-information in the Netherlands. www.dinoloket.nl/en

Van Asselen, S., Erkens, G., Stouthamer, E., Woodlerink, H. A. G., Geeraerts, R. E. E., & Hefting, M. M. (2018). The relative contribution of peat compaction and oxidation to subsidence in built-up areas in the Rhine-Meuse delta, The Netherlands. *Science of the Total Environment*, *636*, 177–191. https://doi.org/10.1016/j.scitotenv.2018.04.141

Van den Biggelaar, D. F. A. M., Kluiving, S. J., Van Balen, R. T., Kasse, C., Troelstra, S. R., & Prins, M. A. (2014). Storms in a lagoon: flooding history during the last 1200 years derived from geological and historical archives of Schokland (Noordoostpolder, the Netherlands). *Netherlands Journal of Geosciences*, *93*, 175–196. https://doi.org/10.1017/njg.2014.14

Van der Meulen, M. J., Van der Spek, A. J. F., De Lange, G., Gruijters, S. H. L. L., Van Gessel, S. F., Nguyen, B.-L., et al. (2007). Regional sediment deficits in the Dutch lowlands: Implications for long-term land-use options. *Journal of Soils and Sediments*, *7*(1), 9–16. https://doi.org/10.1065/jss2006.12.199

Van Dooremolen, W. A., van der Scheer, A., & Winkels, H. J. (1996). Waarnemingen en prognoses van de maaiveldsdaling in Flevoland. Ministerie van Verkeer en Waterstaat, Directoraat-Generaal Rijkswaterstaat, Directie IJsselmeergebied.

Van Hardeveld, H. A., Driessen, P. P. J., Schot, P. P., & Wassen, M. J. (2017). An integrated modelling framework to assess management strategies steering soil subsidence in peatlands. *Environmental Impact Assesssment Review*, *66*, 66–77. https://doi.org/10.1016/j.eiar.2017.06.007

Visschedijk, M. A. T. and Trompille, V. (Eds.) (2009). MSettle Version 8.2. Embankment design and soil settlement prediction. Deltares Report. Retrieved from http://resolver.tudelft.nl/uuid:88aa11df-55a9–4266-89f1-aefb5568dca2

Vos, P. C. (2015). Origin of the Dutch coastal landscape. Long-term landscape evolution of the Netherlands during the Holocene, described and visualized in national, regional and local palaeogeographical map series, (PhD Dissertation, pp. 359). Utrecht University.

Zhao, Q., Lin, H., Gao, W., Zebker, H. A., Chen, A., & Yeung, K. (2011). InSAR detection of residual settlement of an ocean reclamation engineering project: A case study of Hong Kong International Airport. *Journal of Oceanography*, *67*(4), 415–426. https://doi.org/10.1007/s10872-011-0034-3